# *In silico* analyses of substrate interactions with human serum paraoxonase 1

Xin Hu,[1] Xiaohui Jiang,[1] David E. Lenz,[2] Douglas M. Cerasoli,[2] and Anders Wallqvist[1]*

[1] Biotechnology HPC Software Applications Institute, Telemedicine and Advanced Technology Research Center, US Army Medical Research and Materiel Command, Fort Detrick, Maryland 21702

[2] Physiology and Immunology Branch, Research Division, US Army Medical Research Institute of Chemical Defense, Aberdeen Proving Ground, Maryland 21010

## ABSTRACT

Human paraoxonase (HuPON1) is a serum enzyme that exhibits a broad spectrum of hydrolytic activities, including the hydrolysis of various organophosphates, esters, and recently identified lactone substrates. Despite intensive site-directed mutagenesis and other biological studies, the structural basis for the specificity of substrate interactions of HuPON1 remains elusive. In this study, we apply homology modeling, docking, and molecular dynamic (MD) simulations to probe the binding interactions of HuPON1 with representative substrates. The results suggest that the active site of HuPON1 is characterized by two distinct binding regions: the hydrophobic binding site for arylesters/lactones, and the paraoxon binding site for phosphotriesters. The unique binding modes proposed for each type of substrate reveal a number of key residues governing substrate specificity. The polymorphic residue R/Q192 interacts with the leaving group of paraoxon, suggesting it plays an important role in the proper positioning of this substrate in the active site. MD simulations of the optimal binding complexes show that residue Y71 undergoes an "open-closed" conformational change upon ligand binding, and forms strong interactions with substrates. Further binding free energy calculations and residual decomposition give a more refined molecular view of the energetics and origin of HuPON1/substrate interactions. These studies provide a theoretical model of substrate binding and specificity associated with wild type and mutant forms of HuPON1, which can be applied in the rational design of HuPON1 variants as bioscavengers with enhanced catalytic activity.

## INTRODUCTION

Serum paraoxonases (PONs) constitute a family of mammalian enzymes with three members including PON1, PON2, and PON3.[1] PON1 has been intensively studied in past decades owing to its ability to inactivate various organophosphorus compounds such as the nerve agent sarin and the pesticide paraoxon, from which its name was derived historically.[2–4] Human paraoxonase (HuPON1) is a 355-amino acid (43-kDa) glycosylated protein expressed mainly in the liver and is exclusively associated with the "good cholesterol" high-density lipoprotein (HDL).[5] Although the physiological substrate and biological function of HuPON1 are still unclear, studies have shown that it is involved in a wide range of physiologically important hydrolytic activities such as drug metabolism and antiatherosclerosis.[6,7] HuPON1 exhibits a broad spectrum of catalytic activity in the hydrolysis of various substrates, including lactones, thiolactones, carbonates, esters, and phosphotriesters. Recent studies suggested that HuPON1 is most likely a lactonase, whereas the phosphotriesterase and esterase activities can be categorized as "accidental" or "promiscuous."[8–10] A crucial question arises as to how these diverse activities are mediated in HuPON1 and what structural basis and catalytic mechanisms are associated with the hydrolysis of these different substrates.

The three-dimensional structure of a hybrid mammalian recombinant PON1 variant obtained by directed evolution (rePON1) has recently been determined, providing the first structural information on this hydrolase family.[11] The structure revealed a six-bladed β-propeller scaffold resembling the *Loligo vulgaris* diisopropyl fluorophophatase (DFPase),[12] but with unique additions of helices at the top of the propeller forming a closed active site. Two calcium ions are located in the central

tunnel of the propeller; one is buried (termed the "structural calcium"), whereas the solvent-exposed "catalytic calcium" is located at the bottom of the active site. On the basis of substrate titration profiles, a His-His dyad (H115 and H134) in the active site was characterized and postulated to act as a general base and proton shuttle, directly involved in the catalytic mechanism.[10] However, other studies also showed that the H115W mutant of HuPON1 retains activity with paraoxon, arguing that H115 is important for substrate binding and specificity, but does not directly participate in catalysis.[13] Blum *et al.*[14] studied the substrate binding to DFPase and proposed an alternative catalytic mechanism where the calcium coordinating residue D229 in DFPase acts as a nucleophile in the catalytic process. Since an aspartate residue (D269) in HuPON1 is similarly positioned for a nucleophile attack in the PON1 active site, this mechanism may also be part of HuPON1's functionality.

The substrate recognition and catalytic reactions of HuPON1 are considered to be a complex process likely mediated via multiple mechanisms and residues. The three activities of HuPON1 (phosphotriesterase, esterase, and lactonase) have been extensively investigated through kinetic and site-directed mutagenesis studies to delineate substrate specificity. A number of residues have been identified as important for esterase and PON activities, in that substitution of these residues results in diminution or loss of function. These residues include L69, H115, H134, D169, F222, D269, H285, F292, T332, V346, W281, etc.[3,11,15,16] The PON activity of HuPON1, however, is much weaker than the esterase activity. Further studies showed that residues affecting the lactonase/esterase and phosphotriesterase activities seem to be located in different regions of the active site.[17] Although the participation of particular amino acid residues in the activity of HuPON1 can be inferred through directed evolution and mutagenesis experimental studies, a model of the detailed architecture of the catalytic binding site at the atomic level is essential for a better understanding of substrate specificity and catalytic activity. For instance, the HuPON1 R192-polymorphism yields a 10-fold increase in paraoxon hydrolysis, whereas the Q192 form hydrolyzes other substrates, for example, soman and sarin, more rapidly than the R192-polymorph wild type.[18] The lactonase activity is largely retained in HuPON1 variants, but phosphotriesterase and esterase activities are sensitive to mutations.[19] Because HuPON1 is being considered for development as a catalytic bioscavenger of organophosphorus nerve agents, structural insights into the binding interactions of HuPON1 with substrates are important for the design of efficient HuPON1 variants with enhanced phosphotriesterase activity.[3,20,21]

In this article, we performed a detailed computational analysis of HuPON1 interactions with various substrates by means of homology modeling, docking, and molecular dynamic (MD) simulations. HuPON1 is highly similar in amino acid sequence to the recombinant rePON1, allowing a reliable 3D structural model of HuPON1 to be constructed. The binding modes of HuPON1 with phosphotriesters, arylesters, and lactones were probed by docking representative substrates and their analogs into an ensemble of protein conformations. The optimal binding conformation and energetics of the predicted binding complexes with wild-type enzyme and mutants were further investigated by MD simulations and binding free energy calculations. To our knowledge, this is the first theoretical study at the atomic level of HuPON1 in the context of various substrates. The results are in good agreement with experimental observations, providing a detailed molecular model of the structural and energetic determinants of HuPON1 substrate binding and specificity.
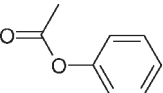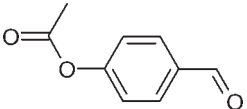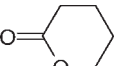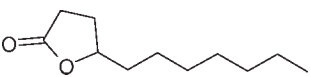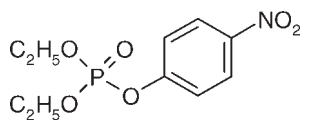
## METHODS

### Substrate compounds

Three types of substrates of HuPON1 (phosphotriesters, arylesters, and lactones) are studied in the present work. Table I shows the representative substrates including phenylacetate, 4-acetoxybenzaldehyde, γ-butyrolactone, γ-undecanoiclactone, δ-valerolactone, and paraoxon. The kinetic parameters of $K_M$, $k_{cat}$, and $k_{cat}/K_M$ were taken from the work of Khersonsky and Tawfik.[9] These experimental data were obtained from the rePON1 variant G2E6.[11] Because the enzymatic properties and biological activities of rePON1-G2E6 are very similar to the wild-type HuPON1, and sequence variations between rePON1-G2E6 and HuPON1 are in regions that do not affect their active sites and overall structure,[11] the experimental data obtained from rePON1 are in general valid for the wild-type HuPON1. Three-dimensional coordinates of all compounds were generated using Sybyl 7.0.[22] A short minimization (500 steepest descent steps with Tripos force field) was performed to remove unphysical internal strains in the molecules.

### Homology modeling

The 3D structural model of HuPON1 was built using the program PSPP package (Protein Structure Prediction Pipeline) developed in our group (http://www.bioanalysis. org/).[23] The PSPP contains a suite of open-source software that predicts protein structures from sequence through the integration of multiple programs including domain boundary detection, sequence homology search, fold recognition, homology modeling, de novo design, and model evaluation. For the HuPON1 modeling, the crystal structure of rePON1 (PDB identifier 1VO4) was used as the template.[11] The disordered loop (72–79) was reconstructed in the modeled structure of HuPON1 by applying spatial restraints and energy minimization. The resulting model was optimized with an iterative approach until no

**Table I**
Data Set of PON1 Substrates Used in this Study

| Name | Structure | $k_{cat}$ $(s^{-1})$ | $K_M$ $(mM)$ | $k_{cat}/K_M$ $(s^{-1} M^{-1})$ |
|---|---|---|---|---|
| Phenylacetate | | 698 | 1.2 | 595,000 |
| 4-Acetoxy benzaldehyde | | 26 | 2.3 | 11,100 |
| γ-Butyrolactone | | 111 | 21 | 5300 |
| δ-Valerolactone | | 210 | 0.57 | 370,000 |
| γ-Undecanoic lactone | | 62 | 0.60 | 103,000 |
| Paraoxon | | 4.8 | 0.8 | 5800 |

Kinetic parameters for substrate hydrolysis by rePON1 were taken from the work of Khersonsky and Tawfik.[9]

significant improvement was obtained. The 3D fold of the generated models was verified by the program PROSA II,[24] and the stereochemical quality and protein structure of the final models were validated by PROCHECK.[25]

## MD simulations

MD simulations were conducted for modeled systems in explicit solvent using the AMBER 9.0 package and the Parm99 force field.[26] The solvated protein systems were subjected to a thorough energy minimization before MD simulations by first minimizing the water molecules while holding the solute frozen (1000 steps using the steepest descent algorithm), followed by 5000 steps of conjugate gradient minimization of the whole system to remove close contacts and to relax the system. Bond lengths involving hydrogen were constrained with SHAKE[27] and the time step for all MD simulations was set to 2 fs. A nonbonded cutoff of 10 Å was used, and the nonbonded pair list was updated every 25 times steps. Periodic boundary conditions were applied to simulate a continuous system. The particle mesh Ewald method was used to calculate the long-range electrostatic interactions.[28] The simulated system was first subjected to a gradual temperature increase from 0 to 300 K over 100 ps, and then equilibrated for 500 ps at 300 K, followed by production runs of 5–10 ns length in total. Constant temperature and pressure (300 K/1 atm) were

maintained using the Berendsen coupling algorithm[29] with a time constant for heat-bath coupling of 0.2 ps. The resulting trajectories were analyzed using the PTRAJ module from the AMBER package. The root-mean-square deviations (RMSDs) of the backbone were calculated from the trajectories at 1 ps interval, with the initial structure as the reference. All MD simulations were carried out at the US Army Research Laboratory Major Shared Resource Center.

## Docking

The AutoDock 4.0 program[30] was applied for docking the substrates to the modeled structure of HuPON1. Multiple conformations associated with residue Y71 and the corresponding flexible loop 72–79 were obtained from MD simulations and used for all docking studies. To avoid artificial steric hindrance of badly placed side chains in the active site, residues Y71 and R192 were treated as flexible during the docking process with Auto-Dock 4.0. For HuPON1 mutants, the corresponding mutated residues were also treated as flexible. The active site of the protein was defined by a grid of 70 × 70 × 70 points with a grid spacing of 0.375 Å centered at the center of mass of the phosphate ligand of the model structure. The Lamarckian Genetic Algorithm in Auto-Dock was applied with 50 runs and the maximum number of energy evaluations was set to 2 × 10⁶. Default

force field parameters for calcium in AutoDock 4.0 was adopted ($r = 0.99$, $\varepsilon = 0.55$). The charge of calcium was set to $+1$ to avoid overestimating its interactions with substrate. All the docking jobs were processed through the DOVIS program developed in our group.[31] Results differing by less than 1.0 Å in positional RMSD of substrate were clustered and the final binding conformations were represented by the one with the most favorable free energy of binding. The optimal binding complexes were subjected a stepwise energy minimization and MD simulations in explicit solvent as described above.

### Binding free energy calculation

The binding free energies were calculated using the MM-GBSA method.[32,33] A set of 300 snapshots was extracted from trajectories of binding complexes at 10 ps intervals from the last 3 ns of each MD simulations. The molecular mechanics interaction energies were calculated with the SANDER module in the Amber 9 package.[26] The polar contribution ($G_{GB}$) was calculated using the generalized Born model by Onufriev *et al.*[34] The same infinite distance cutoff (cut = 999.0) was used in all MM and GB calculations. The nonpolar contributions ($G_{SA}$) were estimated using the MSMS algorithm[35] according to the equation: $G_{SA} = \gamma \times SASA + b$ kcal mol$^{-1}$, with $\gamma$ and $b$ set to 0.00542 kcal/(mol Å$^{-2}$) and 0.92 kcal/mol, respectively, and the probe radius used to calculate the solvent accessible surface area (SASA) was set to 1.4 Å. The entropy (TS) was estimated through normal mode analysis using the NMODE module. Because of the high computational demand, 30 snapshots were used for entropy estimation. Snapshots were selected at equally spaced intervals (100 ps) of the last 3 ns trajectories from each simulation system. Before the normal mode analysis, thorough minimizations were carried out with a distance-dependent dielectric constant ($\varepsilon = 4r_{ij}$, where $r_{ij}$ is the distance between atoms $i$ and $j$) including all non-bonded interactions. Decomposition of the calculated binding free energies was performed using the Amber 9 package.

## RESULTS AND DISCUSSION

### Three-dimensional structural model of HuPON1

Human PON1 shares 86% sequence identity to the recombinant variant (rePON1). Given the high homology to the template structure, the 3D models can be considered reliably constructed.[22] Figure 1 shows a 3D model of HuPON1 in complex with the PO$_4$-ligand. Structural alignment of the HuPON1 model to the template rePON1 exhibited a 0.23 Å of RMSD of the backbone atoms, confirming that the fold is essentially the same. The quality of the modeled structure was also validated
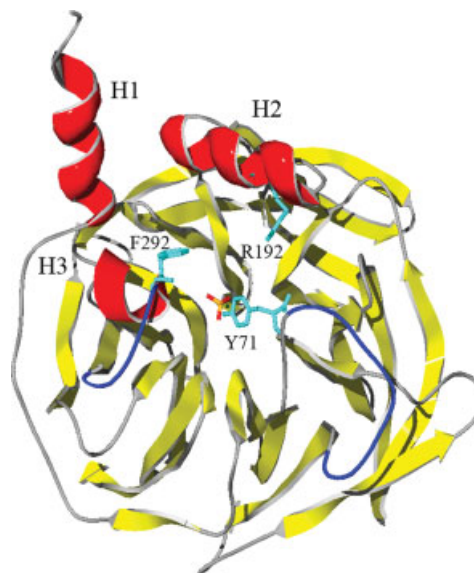


**Figure 1**

The modeled structure of HuPON1. Residues Y71, R192, and F292, as well as the phosphate ion bound in the active site are shown in the "stick and ball" representation. The two flexible loops (L1 and L2) are shown in blue.

with PROCHECK. Ninety-five percent of residues lie in the most favored regions of the Ramachandran plot (100% in allowed region). Likewise, the Z-scores computed by PROSA II are highly comparable to that of the crystal structure of rePON1.

Analysis of the HuPON1 model revealed that structural features observed in rePON1, that is, the six-bladed β-propeller scaffold, the putative catalytic dyad His115-His134 in the active site, the calcium-ligating residues centered in the tunnel, and the three helices at the top of the propeller are well conserved in HuPON1. The phosphate ion modeled in HuPON1 was bound to the catalytic calcium in the same manner as observed in the structure of rePON1. Helices H1 and H2 exhibit major sequence variations between HuPON1 and rePON1, but most of these mutated residues are located on the protein surface. The hydrophobicity of the N-terminal helix H1, which is presumably associated with HDL binding, is also retained. Residues defining the active site of HuPON1 are generally identical to those of rePON1, with the exception of K192, which is normally R/Q in HuPON1. A previously reported model structure of HuPON1 (PDB code 1XHR) was based on a template of DFPase.[21] In comparison with this structure, the β-propeller folding motifs agree well, but the three helices that are essential for the formation of the catalytic site are missing from the DFPase-derived model, resulting in significant discrepancies among key residues in the active site.
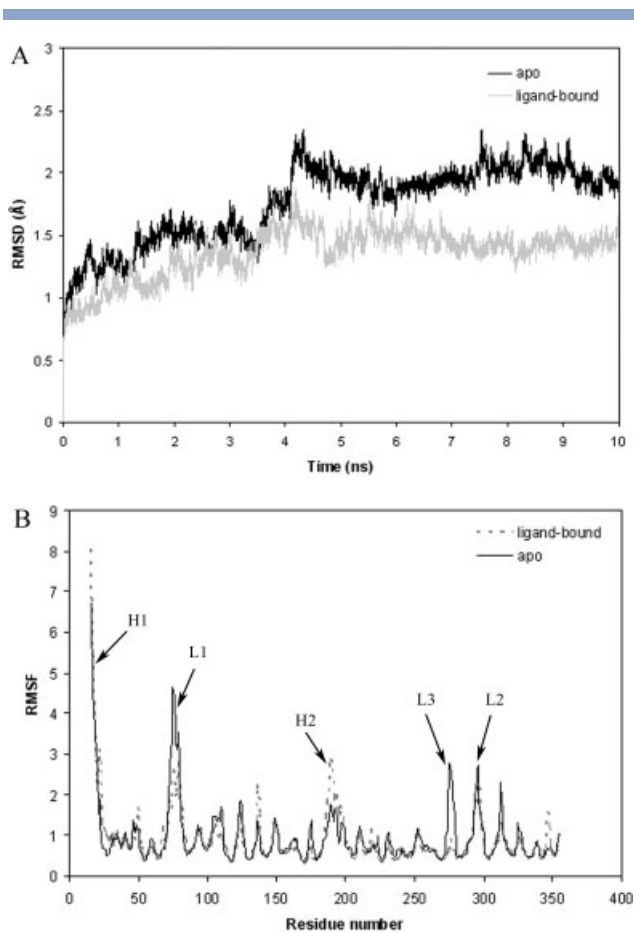
**Figure 2**

(**A**) RMSDs calculated for the backbone atoms of protein over a time course of 10 ns for the two simulated systems. (**B**) The calculated fluctuations of CA backbone atom (RMSF) of HuPON1 for the simulations of the apo and complexed HuPON1 systems.

## Dynamics of HuPON1

To gain insight into the stability and dynamic properties of the HuPON1 structure, we performed explicit solvent MD simulations of both the apo form and the phosphate ligand-bound complex. Figure 2A shows the plots of RMSDs calculated for the backbone atoms of the two simulated systems over a time course of 10 ns. The ligand-bound complex displayed a stable plateau after 2-ns of simulations with an averaged RMSD value less than 1.5 Å, whereas the RMSD of the apo form deviated more with an abrupt change at ~4 ns. At this point the RMSD increased from an average of 1.5 to 2.0 Å, indicating a conformational transition. To detect local structure motions, the fluctuations of backbone atom CA were calculated from the simulation trajectories. As shown in Figure 2B, both apo and ligand-bound proteins exhibited significant fluctuations within the regions surrounding the active site, reflecting the flexibility of the catalytic binding site of HuPON1. Except for the

N-terminal tail of H1, loop 72–79 (designed as L1 in this article) exhibited the highest level of fluctuations throughout the MD simulations. This is consistent with the disordered form of this loop observed in the crystal structure of rePON1. In addition, the H3-extended loop 292–300 (designed as L2) also exhibited high fluctuation in the simulations. Both loops L1 and L2 are located at the front of the active site, forming a tunnel entrance to the binding pocket. Therefore, the high flexibility of these loops might play a selectivity-determining role in substrate recognition.[4] In comparison with the apo form, atomic fluctuations in the ligand-bound form were significantly decreased, especially for loop L1. The motion of a small loop L3 (175–278) on the back of the active site was found to be highly correlated with loop L2 in the apo form, and also stabilized upon ligand binding. However, helix H2 became more mobile in the ligand-bound state, implying that the dynamic effects of ligand binding are mediated differently across the active site.

A detailed trajectory analysis revealed that the active site in the apo form undergoes a "closed-open" conformational change associated with the flexible loop L1 and residue Y71. Figure 3 shows the changes of the torsion angle of the Y71 side-chain over the time course of the simulation, with representative snapshots extracted from the trajectories. The closed conformation, characterized by Y71 pointing into the active site, was predominately observed with the phosphate-bound complex. It remained stable over the entire simulation due to the formation of a hydrogen bond between the OH group of Y71 and the phosphate ligand. In contrast, the closed Y71 conformation in the apo form was retained only in the early stage of the simulation. The increased fluctuations of loop L1 in the apo form caused a distinctive conformational change of Y71 with the side-chain pointing away from the active site, resulting in an open conformation (Fig. 3B). The open conformation in the apo state was stabilized by the H-bonding interaction between the OH group of Y71 and the guanidino group of R192, which seems to be more energetically preferred. A short period of transition from "open" to "closed" form was also observed at ~9 ns, indicating that the free energy barrier between the two conformations is rather low. The flexible transition of Y71, and the plasticity of the active site, may be of importance for HuPON1 substrate binding, as delineated in the sections below.

## HuPON1/ester interaction

With the modeled 3D structure of HuPON1, we docked the arylester substrate phenylacetate into the active site by taking into account multiple conformations associated with loop L1 and residue Y71. The most favorable binding conformation predicted by AutoDock is shown in Figure 4A. Several interesting features can be identified from this binding complex. The substrate binds
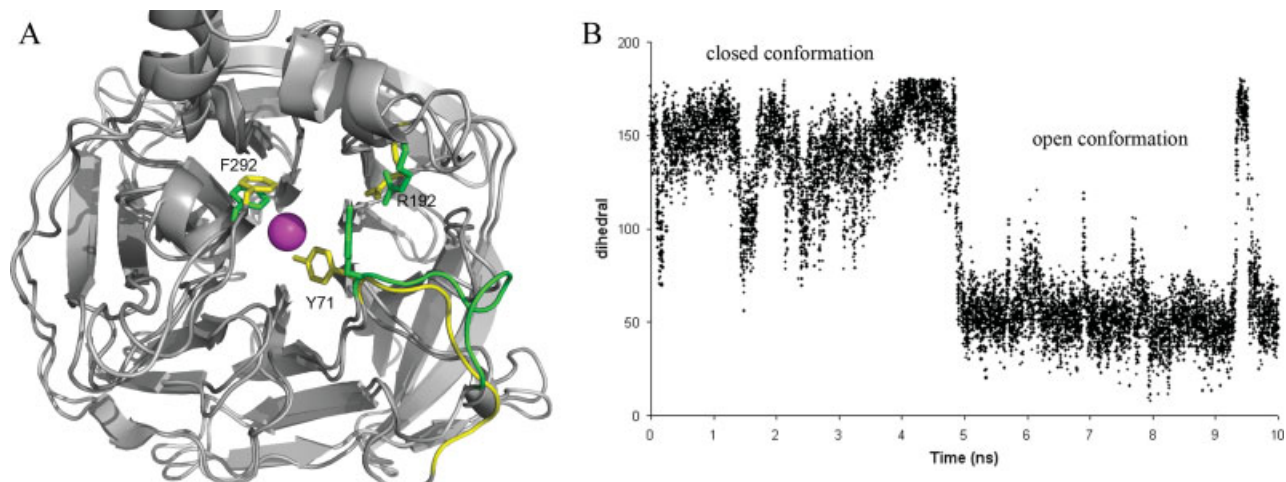
**Figure 3**

(**A**) Overlay of the open and closed conformations of HuPON1 observed in the MD simulations. Residues Y71, R192, and F292 are shown in sticks (yellow in the closed conformation, green in the open conformation). The calcium ion is shown as a magenta colored sphere. (**B**) The plots of the torsion angles of Y71 side-chain over the time course of 10-ns simulations of HuPON1.

in the hydrophobic pocket of the active site and forms extensive hydrophobic and aromatic stacking interactions with a number of residues including I291, F292, Y294, T332, and V346. Most of these residues have been found to be associated with esterase activity of HuPON1 from site-direct mutagenesis studies.[11] The carboxyl oxygen of phenylacetate binds to the catalytic calcium atom in the "oxyanion hole" at a distance of 2.81 Å. The "catalytic residue" H115 is located on the other side, pointing to the substrate with a distance of 4.38 Å between the ε-N of imidazole and the carbonyl carbon atom. This binding orientation seems to be essential for the catalytic attack

via a water molecule, as proposed by Harel *et al.*,[11] by mimicking the oxyanionic moiety of the reaction intermediate and stabilizing the charged complex.

Notably, residue Y71 adopts a closed conformation in the docked complex, pointing into the active site as was observed in the crystal structure of rePON1. To further characterize the dynamic behavior of phenylacetate interactions with HuPON1, we performed explicit solvent MD simulations for the bound complex. The results showed that residue Y71 underwent a conformational transition from the closed form to an open state; similar to what was observed in the apo form. In Figure 5, the
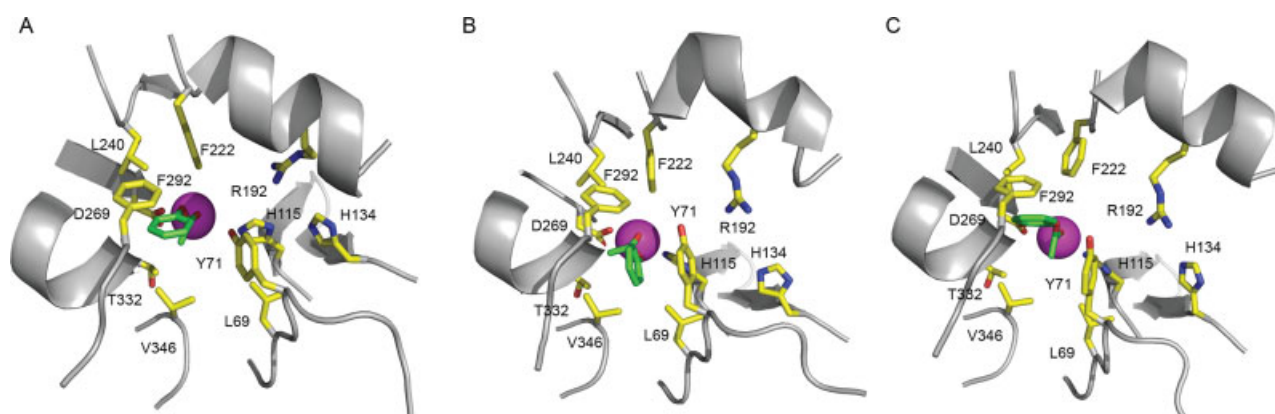


**Figure 4**

(**A**) The closed binding conformation of phenylacetate with HuPON1 predicted by AutoDock. (**B**) The intermediate binding conformation of phenylacetate with HuPON1 observed in MD simulations. (**C**) The open binding conformation of phenylacetate with HuPON1 observed in MD simulations. The phenylacetate substrate is shown in green, the side chain of active site residues are shown in sticks (yellow) with backbone shown in ribbon (grey), and calcium ion is shown as a magenta-colored sphere.
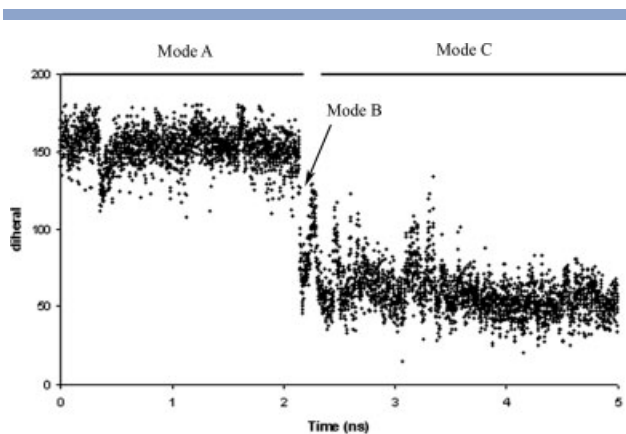
**Figure 5**

The torsion angel of the side chain of Y71 taken from the 5-ns MD simulations of HuPON1/phenylacetate binding complex. Mode A represents the closed conformation of Y71, and Mode C represents the open conformation of Y71. Mode B indicates an "intermediate" conformation between the transitions that last for ~200 ps.

change in the torsion angle of the side chain of Y71 indicates the opening of the active site at ~2 ns. The open binding conformation remained stable over the rest of simulation time. It is likely that the open conformation is more energetically preferred due to favorable binding interactions. As shown in Figure 4C, phenylacetate binds to the hydrophobic pocket in the same manner as that of the closed conformation, forming an aromatic stacking interaction with F292. A major difference is that residue Y71 adopts an open conformation compared with the initial, closed state. As a result, the open Y71, together with L240, F222, and F292, form a hydrophobic cavity for the substrate. In addition, the OH group of Y71 could stabilize the open binding conformation by forming a hydrogen bond with both R192 and the substrate, thus contributing significantly to the binding affinity. Trajectory analysis showed that phenylacetate bound in the active site also undergoes a significant conformational change during the opening of Y71 (see Fig. 5). This "intermediate" binding conformation, which lasts for ~200 ps, is characterized by the substrate phenyl ring positioned in a perpendicular manner that faces the side chain of Y71 and forms an aromatic stacking interaction (Fig. 4B). In comparison with the open conformation, the "intermediate" binding mode does not seem to be well accommodated within the hydrophobic pocket, as the stacking and hydrophobic interactions between the substrate and residues F292, F222, and L240 are mostly disrupted.

Because phenylacetate is positioned towards the entrance of the narrow hydrophobic pocket and thus provides room for bulky substituents, the "intermediate" conformation likely represents an optimal binding mode for the analogs of phenylacetate substrates. To validate

this hypothesis, we docked 4-acetoxybenzaldehyde into the active site and analyzed the energetically favorable binding conformations. As expected, the binding of this analog to the hydrophobic region is similar to the "intermediate" binding mode of phenylacetate (see Fig. 6). The phenyl ring faces the aromatic side chain of Y71, allowing the acetoxyl substitute to protrude from the hydrophobic binding pocket. The para-substitute of the acetoxyl group may cause steric hindrance within the pocket, especially with the "lid" formed by residue F292, preventing binding more deeply in the pocket. MD simulations revealed that the 4-acetoxybenzaldehyde binding complex remains stable and no significant conformation changes were observed.

### HuPON1/lactone interaction

Recent studies strongly suggest that lactones are the natural substrate of PON1, with kinetic behavior different from other substrate classes.[8,9] The rate of hydrolysis of lactones is substantially dependent on the $K_M$ values, whereas this is not the case for esters and paraoxon. For a six-member ring containing δ-valerolactone, the $K_M$ is ~50 times lower than that of a five-member ring containing γ-butyrolactone. Ring substituents of γ-butyrolactone, such as γ-undecanoiclactone, increase the binding affinities proportionally to the length of the aliphatic substituents, resulting in dramatic difference in $k_{cat}/K_M$ values.[9] To probe the underlying atomic nature of these substrate binding interactions, we docked various lactones to the modeled structure of HuPON1 and
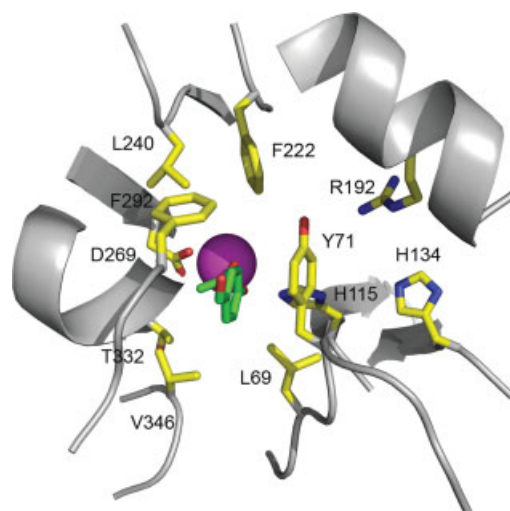


**Figure 6**

The binding conformation of 4-acetoxybenzaldehyde with HuPON1 as predicted by AutoDock. The substrate is shown in green, the side chain of active site residues are shown in sticks (yellow) with backbone shown in ribbon (grey), and the calcium ion is shown as a magenta-colored sphere.

**Figure 7**

The binding conformation of γ-butyrolactone (**A**), δ-valerolactone (**B**), and γ-undecanoiclactone (**C**) with HuPON1 as predicted by AutoDock. The substrate is shown in green, the side chain of active site residues are shown in sticks (yellow) with backbone shown in ribbon (grey), and the calcium ion is shown as a magenta-colored sphere.
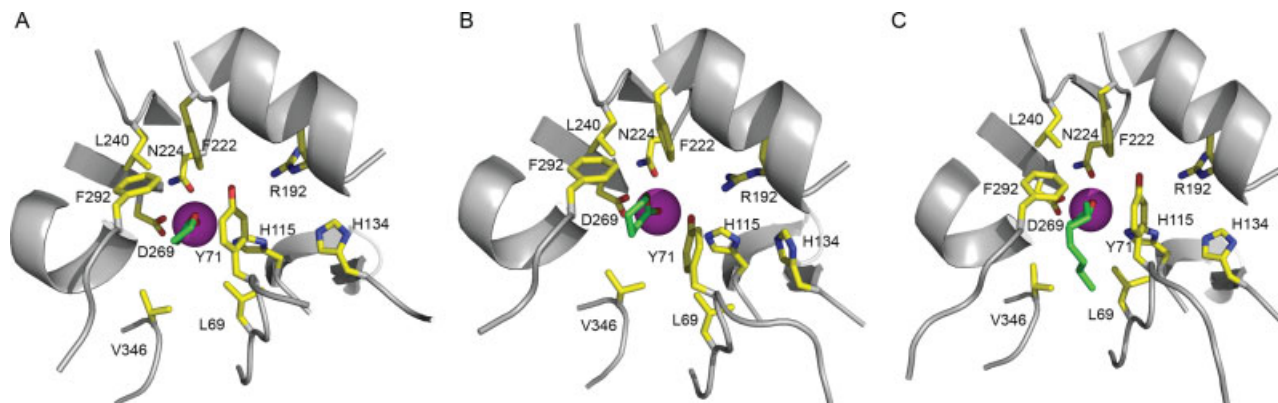
performed MD simulations of the bound complexes. The binding modes of γ-butyrolactone, δ-valerolactone, and γ-undecanoiclactone are shown in Figure 7. Similar to the arylester phenylacetate, the small lactone substrates γ-butyrolactone and δ-valerolactone are well accommodated in the hydrophobic pocket of the active site, implying that lactone binding is also driven by hydrophobic interactions. The five/six-member ring of γ/δ-lactones is positioned in such a way that it is perpendicular to the phenyl ring of F292, forming stacking interactions with the open form of Y71 [Figs. 7(A,B)]. The long aliphatic substituents of γ-undecanoiclactone protrudes from the pocket into the hydrophobic tunnel, participating in extensive hydrophobic interactions with residues along the tunnel wall, for example, Y294 and F347 (Fig. 7C).

Unlike the phenylacetate substrate bound in HuPON1, the perpendicular binding orientation of the five- or six-member ring would allow the alkoxy-atom to point upwards and form hydrogen bonds with residues N224 and N168. MD simulations of the two complexes showed that the binding conformation of δ-valerolactone is quite stable with the hydrogen bonding interactions maintained. In contrast, γ-butyrolactone exhibited large fluctuations with the 5-member ring flapping up and down intermittently during the simulations. In fact, besides the intrinsic properties and the size of the ring involved in the hydrophobic interactions, the higher experimental binding affinities of δ-valerolactone over γ-butyrolactone (0.59 vs. 21 m$M$ for $K_M$, respectively)[9] are probably due to the well-defined H-bonding network with the calcium-ligating residues. Notably, with the addition of ring substituents, the stability of the binding interactions of γ-undecanoiclactone was significantly increased. This is evident from the enhanced binding affinities of γ-undecanoiclactone and lack of steric hindrance along the

hydrophobic tunnel in the predicted binding complex (Fig. 7C).

### HuPON1/phosphotriester interaction

Figure 8A shows the predicted binding mode of paraoxon in HuPON1. Several distinguishing binding features can be identified with the optimal paraoxon/HuPON1 interaction. First, paraoxon is orientated in a different region in the active site, opposite to the hydrophobic binding pocket used by ester and lactone substrates. This paraoxon binding site is mainly formed by helix H2 and loop L1, with the postulated catalytic residues H115 and H134 located at the bottom. A number of residues within this site, such as R192, S193, and F222, are known to be involved in PON activity.[13,21] Second, the paraoxon substrate is situated on top of the proposed catalytic histidine dyad, while the phosphate group is pointing to the catalytic calcium atom facing residue D269. Such a binding mode is consistent with the recently proposed catalytic mechanism in which D269 serves as the catalytic residue for nucleophile attack in the hydrolysis of phosphotriester substrates, rather than the His dyad used by esters and lactones.[13] Third, the leaving group of the nitrophenyl moiety is directed towards residue R192, potentially engaged in ionic and hydrogen bonding interactions with the positively charged guanidino group. This interaction provides a plausible rational for the well-established difference in activity of the polymorphisms R192Q, wherein the R has significantly increased PON activity compared with the Q form.[18] By this model, the binding affinity of the nitrophenyl group of paraoxon with the positively-charged R192 would be much stronger compared to that with neutral Q192. The estimated binding free energies of paraoxon with the two R192 and
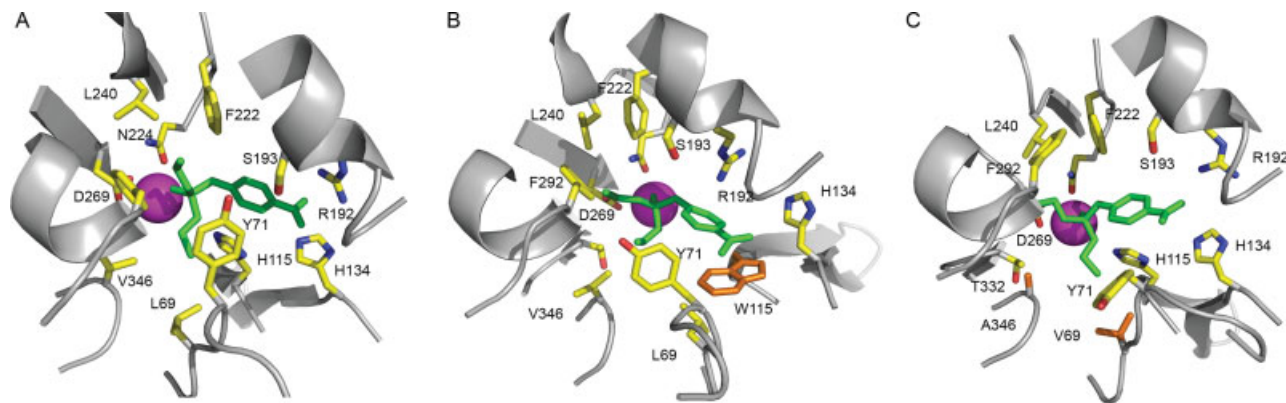
**Figure 8**

The binding conformation of paraoxon with wild-type HuPON1 (**A**), H115W mutant (**B**), and L69V/V346A mutant (**C**) as predicted by AutoDock. The substrate is shown in green, the side chain of active site residues are shown in sticks (yellow) with backbone shown in ribbon (green). Mutated residues (W115, V69, and A346) are shown in brown. The calcium ion is shown as sphere in magenta.

Q192 variants as calculated with AutoDock are −3.69 and −3.40 kcal/mol, respectively. More significantly, the favorable binding interaction with R192 would facilitate the proper positioning of the substrate in the active site. This is critical to the PON activity, as steric hindrance and inadequate positioning of the phosphotriester substrates seem to be major factors for their observed low $k_{cat}$ values.[9] Finally, residue Y71 adopts a more open conformation in the binding complex with paraoxon. This is essential for paraoxon bound in the active site of HuPON1, as the closed form of Y71 would cause significant steric interference with the substrate. MD simulations and binding free energy calculation indicate that Y71 plays an important role in paraoxon binding, and makes significant contribution to the estimated binding free energies (discussed below).

A comparison of paraoxon and phenylacetate docked to HuPON1 mutants provides structural insights into the relative activities of HuPON1 with each substrate. Experiments show that the F222Y mutation abolished the PON activity of HuPON1 but retained the esterase activity, with a 1.5-fold increase in $K_M$ for phenylacetate. However, replacing phenylalanine with aspartate (F222D) abolished both esterase and PON activity.[13,21] As seen in Figure 8A, F222 is located on the top of the binding pocket and points to the paraoxon binding site. When paraoxon binds to the F222Y mutant, the substituted residue apparently causes steric hindrance and prevents the substrate from inserting into the catalytic site. In contrast, for the phenylacetate substrate, no significant steric hindrance is predicted. The elimination of both esterase and PON activities in the F222D mutant is consistent with the mutated aspartate residue creating an unfavorable electrostatic interaction with the substrates and destabilizing the positively-charged binding center. Although the effects of mutations at F222 on lactonase activity

have not been reported, we postulate that this activity would also be abolished with the F222D mutant, whereas the effect would be less significant for the F222Y mutant.

To further investigate the impact of amino acid substitutions, we modeled the binding interactions of paraoxon with HuPON1 mutants H115W, L69V, and V346A. The PON activity of these mutants has been extensively studied, and the results showed a ∼2 fold increase for H115W, and ∼4–16 fold higher PON activity for the V346A and L69V mutants.[11,21] The predicted binding modes of paraoxon with H115W show that the mutated residue adopts a conformation with the indole side chain parallel to the nitrophenyl group of paraoxon, thus forming a cluster of strong aromatic stacking interactions (Fig. 8B). For the mutant L69V/V369A, the docked complex suggests that the binding of the ethyl group of paraoxon, which points to the bottom of the active site, seems to be energetically favored by the enlarged hydrophobic pocket formed by the mutated residues A346 and V69 (Fig. 8C). The increased binding affinities of paraoxon to the mutant enzymes are also mimicked by the calculated AutoDock binding free energies, as being −4.54 kcal/mol for H115W, and −4.19 kcal/mol for L69V/V346A, when compared with the wild-type binding energy of −3.69 kcal/mol.

## Binding free energy decomposition

To gain further insight into the structural basis and energetics of substrate interactions, we calculated binding free energies using the MM-GBSA method, and decomposed energetic components into individual ligand-residue pair.[32,33] This allowed us to estimate the contribution of each residue to the binding affinity, and to pinpoint residues important for determining substrate specificity. The calculated binding free energies for the

**Table II**
Binding Free Energies of HuPON1 (R192) with Substrates Phenylacetate, γ-Undecanoiclactone, and Paraoxon Calculated by MM-GBSA

| Substrate | $\Delta E_{elec}$ | $\Delta E_{vdw}$ | $\Delta G_{nonpol}$ | $\Delta G_{polar}$ | $-T\Delta S$ | $\Delta G_{pred}$ | $\Delta G_{exp}$ |
|---|---|---|---|---|---|---|---|
| Phenylacetate | −11.19 (2.81) | −20.99 (2.16) | −3.12 (0.11) | 18.80 (2.68) | 13.92 (7.61) | −2.57 | −4.39[a], −3.98[b] |
| γ-Undecanoiclactone | −4.25 (2.67) | −25.00 (3.36) | −3.97 (0.26) | 12.61 (2.88) | 15.60 (5.86) | −5.01 | −4.39[b] |
| Paraoxon | −46.49 (6.78) | −35.33 (3.57) | −4.91 (0.12) | 58.58 (4.09) | 18.93 (7.45) | −9.23 | −5.18[a], −4.22[b] |

The predicted free energies ($\Delta G_{pred}$) are the sums of the contributions ($\Delta E_{elec}$, $\Delta E_{vdw}$, $\Delta G_{nonpol}$, $\Delta G_{polar}$, and $-T\Delta S$). All values are given in kcal/mol. The standard deviations are shown in parenthesis.
[a]Experimental data ($K_M$) by HuPON1 (Q192) taken from the work of Yeung and Cerasoli.[21]
[b]$K_M$ by rePON1 taken from the work of Khersonsky and Tawfik.[9]

three substrates are shown in Table II, whereas Figure 9 depicts the binding free energy contributions of key residues identified in terms of electrostatic, van der Waals interactions, and changes in solvation. Overall, the van der Waals interactions and the nonpolar part of solvation free energies are predominately favorable for the binding of phenylacetate and lactones, whereas for paraoxon both van der Waals and electrostatic interactions contribute favorably to the binding energies. These results are consistent with our previous binding analysis, in which the more favorable electrostatic interactions observed in paraoxon binding are mostly due to the interactions with R192, as revealed by the energy decomposition shown in Figure 9. The estimated binding free energies for the three substrates are generally in fair agreement with the experimental data that was obtained from recombinant Q192-HuPON1 and the rePON1 variants (Table II). The predicted binding affinities are expected to be higher than those for Q192-HuPON1 because the variant used in our calculation is R192-HuPON1, and experimental data show a ~10-fold increase of paraoxon activity for R192.[18]

A number of residues important for substrate interaction were identified from the binding free energy decomposition. With a free energy cutoff of 0.1 kcal/mol to indicate binding of a residue to the substrate, 18 residues are predicted to participate in phenylacetate binding, 16 in lactone binding, and 24 in paraoxon binding (see Fig. 9). These "binding epitopes" associated with the binding of each substrate can generally be categorized as the first shell calcium-ligating residues (E53, D269, N168, N224, and N270), hydrophobic pocket-forming residues (L240, V346, F292, I291, F222, L69, H115, H285, T332, L267, and F347), and paraoxon-binding residues from helix H2 and loop L1 (Y71, P72, R192, L191, M196, D188, and P189). Most of these residues have been extensively studied with mutagenesis experiments, showing a range of effects on substrate specificity. For phenylacetate and γ-undecanoiclactone, the majority of residues contributing to binding energies lie in the hydrophobic pocket. Residue L240 contributes −1.24 kcal/mol to phenylacetate binding, whereas F292 contributes −2.08 kcal/mol to γ-undecanoiclactone binding. Both are key residues positioned on top of the substrate as observed from the predicted binding complexes (Figs. 4A and 7C). For para-

oxon binding, Y71 is the largest contributing residue (−2.71 kcal/mol), followed by the calcium-ligating residue E53 (−2.15 kcal/mol) and R192 (−2.07 kcal/mol). These residues form the major interactions with the phenyl ring, the phosphate group, and the nitro group of the paraoxon substrate (Fig. 8A). It is worth noting that Y71 is also a large contributor to the binding of lactones (−1.95 kcal/mol), and for interactions with phenylacetate (−0.75 kcal/mol). These results are consistent with our binding mode analysis, reiterating the potential importance of Y71 in substrate interactions. Interestingly, the first shell calcium-ligating residues contribute more to the binding of phenylacetate and paraoxon than to lactone binding.

As an alternative to the experimental/computational alanine scanning method,[36] binding free energy decomposition provides a means to rapidly estimate mutational effects and guide the experimental design of site-directed mutagenesis efforts. As discussed above, residue Y71 seems to be a candidate for experimental mutation. Useful information may also be gained from examining the contributions of residues in terms of electrostatic interactions, van der Waals interactions, and solvation energy contributions. For example, for those residues predicted to have unfavorable electrostatic interactions with paraoxon, for example, P189, T332, N270, D188 (Fig. 9 and supporting Tables S1–S3), mutations to nonpolar residues could be considered. D188 is a surface residue located on H2 distal from the catalytic site. It is potentially involved in paraoxon binding through interaction with the nitrophenyl group. Hence, mutation of this residue to lysine or arginine, together with the neighboring P189 mutation (e.g., to alanine, leucine, or arginine), could effectively improve paraoxon binding. The binding free energy can further be analyzed in terms of energy contributions from both backbone and side chain atoms. As shown in Figure 10, the side chain of D183 seems to disfavor paraoxon binding due to its charged nature and possible electrostatic repulsion with the phosphate group of paraoxon. Therefore, the mutation D183N might improve the binding affinity of HuPON1 for organophosphate substrates. Similarly, the side chain of S193 is not predicted to make any contribution to the binding energy, and likely generates unfavorable polar solvation
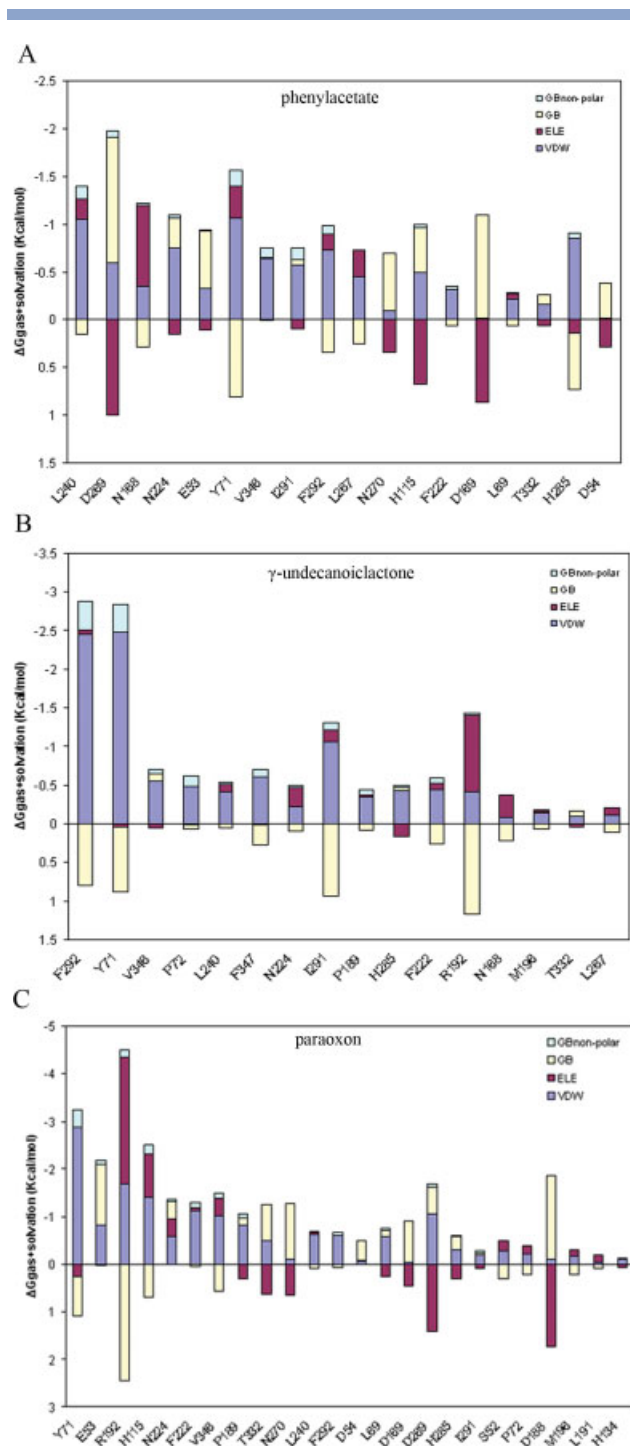
energies (Supporting Table S3). This is consistent with the experimental observation that the S193P mutant increases phosphotriesterase activity.[11]

## Implications for the catalytic mechanism

Figure 11A depicts the overall architecture of the active site of HuPON1 in the context of substrate binding interaction. It is evident from our modeling analysis that the binding site is characterized by two distinct regions on the sides for substrate interactions: the hydrophobic binding site for arylesters/lactones, and the paraoxon binding site for phosphotriesters. A well-defined hydrophobic pocket is formed on the side of helix H3, mainly consisting of residues I291, F292, Y294 from the H3-extended loop L2, residues L240, F222 on the top, and T332, V346 at the bottom of the active site. This hydrophobic region is typically associated with the lactonase and esterase activities of HuPON1 from mutagenesis studies.[17] On the other hand, the opposite side is primarily composed of polar residues, for example, R192 and S193 from helix H2, and Y71 from the flexible loop L1. Experiments have shown that PON activity is sensitive to amino acid substitutions in this region.[17]

Our predicted models for substrate binding support the proposed catalytic mechanisms of HuPON1 associated with each type of substrate.[11,14,17] Figure 11B shows the superposition of the three substrates (phenylacetate, δ-valerolactone, and paraoxon) bound in the active site of HuPON1. Except for the difference in binding orientation of the phenyl and six-member ring (parallel vs. perpendicular), phenylacetate and δ-valerolactone bind in the hydrophobic site in the same manner with the carbonyl group pointing towards the proposed
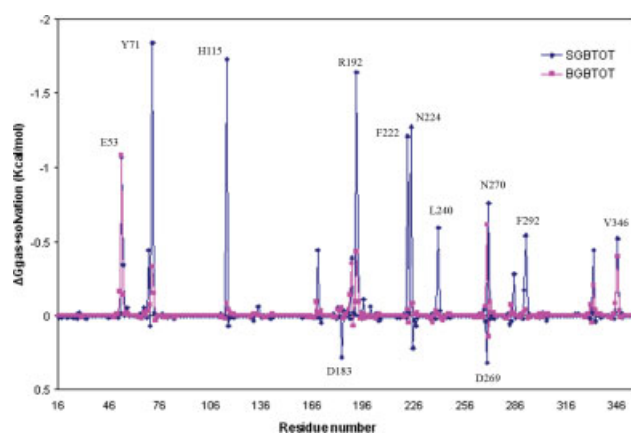
**Figure 9**

The substrate binding free energy contributions of key active-site residues of HuPON1 for phenylacetate (**A**), γ-undecanoiclactone (**B**), and paraoxon (**C**). The residues were selected based on an interaction energy cutoff of 0.1 kcal/mol. The residue binding free energies are decomposed into individual terms based on the MM-GBSA calculations (see supporting materials for further details). [Color figure can be viewed in the online issue, which is available at www.interscience. wiley.com.]



**Figure 10**

The residue-based binding free energy contributions of the backbone (red) and side chain (blue) for paraoxon bound HuPON1 (see supporting Tables S1–S3 for further details). [Color figure can be viewed in the online issue, which is available at www.interscience. wiley.com.]
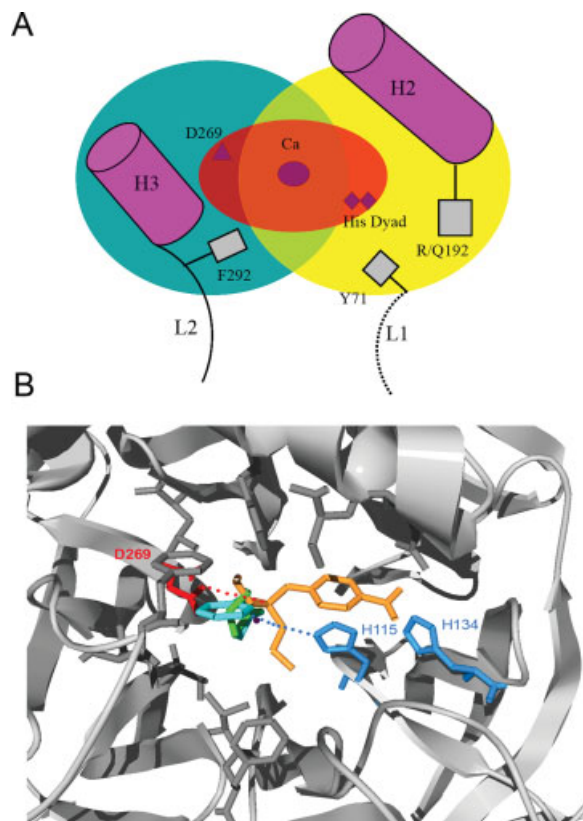
**Figure 11**

(**A**) A schematic representation of the overall architecture of the active site of HuPON1. The ester/lactone binding region (in cyan) and paraoxon binding region (in yellow) are shown as circles, and the calcium-ligating center with postulated catalytic residues His dyad and D269 are shown in the red region. Active-site associated helices (H2 and H3) and loops (L1 and L2), as well as residues (R192, F292, and Y71), are also illustrated. (**B**) Superposition of three substrates phenylacetate (cyan), δ-valerolactone (green), and paraoxon (yellow) bound in the active site of HuPON1. The proposed catalytic residues are also shown in color (His dyad in blue, D269 in red).

catalytic His dyad, implying that ester- and lactone-substrate binding adopt a similar catalytic mechanism mediated by the His dyad and a water molecule.[11,17] In contrast, the main part of the paraoxon molecule predominantly occupies the polar binding region in the active site, with the phosphate group pointing towards the catalytic residue D269. Interestingly, MD simulations show that the distances between the substrate ester/lactone carbonyl carbon atom and H115 (ε-N of imidazole) remain stable ($\sim$4 Å), whereas the distance between the D269 carboxyl oxygen atom and the phosphorous atom of paraoxon varied between 4.8 and 3.5 Å (Supporting Fig. S4). In Figure 10 the predicted binding free energy decomposition indicates that the side chain of D269 negatively impact paraoxon binding. It is postulated that the carbonyl group of D269 may act in a direct nucleophilic attack on the phosphorus atom of paraoxon in the cata-

lytic process generating a high-energy phosphor-enzyme intermediate.[14] The unfavorable interactions of the D269 side chain with paraoxon seem to be compatible with a high-energy intermediate required for this nucleophilic attack. Probing such catalytic mechanisms involving bond-breaking and bond-formation, however, is a more challenging problem requiring high level quantum mechanical calculations.

## CONCLUSIONS

Structural information describing HuPON1 substrate interactions is of primary importance in the development of effective HuPON1 variants as bioscavengers. In the present study, we have constructed a three-dimensional structural model of HuPON1 and probed binding interactions of HuPON1 with various substrates (esters, lactones, and phosphotriesters) using molecular docking, MD simulations, and binding free energy calculations. We have delineated dynamic characteristics of the active site of HuPON1 and predicted optimal binding conformations associated with each type of substrate. The proposed binding modes and a number of key residues identified from binding free energy decomposition supported the conclusion that different amino acid residues in HuPON1 contribute to substrate binding, specificity, and postulated catalytic mechanisms, depending on the class of substrate modeled. Of importance, residue Y71 is highly associated with binding of all three modeled substrates. It is likely that this residue is involved in the catalytic process, serving as a gate in the active site to facilitate substrate recognition. In conjunction with these computational studies, we are currently undertaking site-directed mutagenesis studies of this and many other amino acid residues. Taken together, these studies shed light on the structural basis for substrate interaction and catalytic mechanisms associated with HuPON1, and provide a rationale for further engineering of this enzyme as a catalytic bioscavenger.

## ACKNOWLEDGMENTS

## REFERENCES

1. Draganov DI, La Du BN. Pharmacogenetics of paraoxonases: a brief review. Naunyn Schmiedebergs Arch Pharmacol 2004;369:78–88.
2. Main AR. The differentiation of the A-type esterases in sheep serum. Biochem J 1960;75:188–195.

3. Lenz DE, Yeung D, Smith JR, Sweeney RE, Lumley LA, Cerasoli DM. Stoichiometric and catalytic scavengers as protection against nerve agent toxicity: a mini review. Toxicology 2007;233:31–39.

4. Rochu D, Renault F, Clery-Barraud C, Chabriere E, Masson P. Stability of highly purified human paraoxonase (PON1): association with human phosphate binding protein (HPBP) is essential for preserving its active conformation(s). Biochim Biophys Acta 2007; 1774:874–883.

5. Sorenson RC, Bisgaier CL, Aviram M, Hsu C, Billecke S, La Du BN. Human serum paraoxonase/arylesterase's retained hydrophobic N-terminal leader sequence associates with HDLs by binding phospholipids: apolipoprotein A-I stabilizes activity. Arterioscler Thromb Vasc Biol 1999;19:2214–2225.

6. La Du BN, Aviram M, Billecke S, Navab M, Primo-Parmo S, Sorenson RC, Standiford TJ. On the physiological role(s) of the paraoxonases. Chem Biol Interact 1999;119–120:379–388.

7. Fuhrman B, Volkova N, Aviram M. Oxidative stress increases the expression of the CD36 scavenger receptor and the cellular uptake of oxidized low-density lipoprotein in macrophages from atherosclerotic mice: protective role of antioxidants and of paraoxonase. Atherosclerosis 2002;161:307–316.

8. Draganov DI, Teiber JF, Speelman A, Osawa Y, Sunahara R, La Du BN. Human paraoxonases (PON1, PON2, and PON3) are lactonases with overlapping and distinct substrate specificities. J Lipid Res 2005;46:1239–1247.

9. Khersonsky O, Tawfik DS. Structure-reactivity studies of serum paraoxonase PON1 suggest that its native activity is lactonase. Biochemistry 2005;44:6371–6382.

10. Aharoni A, Gaidukov L, Khersonsky O, Mc QGS, Roodveldt C, Tawfik DS. The 'evolvability' of promiscuous protein functions. Nat Genet 2005;37:73–76.

11. Harel M, Aharoni A, Gaidukov L, Brumshtein B, Khersonsky O, Meged R, Dvir H, Ravelli RB, McCarthy A, Toker L, Silman I, Sussman JL, Tawfik DS. Structure and evolution of the serum paraoxonase family of detoxifying and anti-atherosclerotic enzymes. Nat Struct Mol Biol 2004;11:412–419.

12. Scharff EI, Koepke J, Fritzsch G, Lucke C, Ruterjans H. Crystal structure of diisopropylfluorophosphatase from *Loligo vulgaris.* Structure 2001;9:493–502.

13. Yeung DT, Lenz DE, Cerasoli DM. Analysis of active-site amino-acid residues of human serum paraoxonase using competitive substrates. FEBS J 2005;272:2225–2230.

14. Blum MM, Lohr F, Richardt A, Ruterjans H, Chen JC. Binding of a designed substrate analogue to diisopropyl fluorophosphatase: implications for the phosphotriesterase mechanism. J Am Chem Soc 2006;128:12750–12757.

15. Josse D, Lockridge O, Xie W, Bartels CF, Schopfer LM, Masson P. The active site of human paraoxonase (PON1). J Appl Toxicol 2001;21(suppl 1):S7–S11.

16. Josse D, Xie W, Masson P, Lockridge O. Human serum paraoxonase (PON1): identification of essential amino acid residues by group-selective labelling and site-directed mutagenesis. Chem Biol Interact 1999;119–120:71–78.

17. Khersonsky O, Tawfik DS. The histidine 115-histidine 134 dyad mediates the lactonase activity of mammalian serum paraoxonases. J Biol Chem 2006;281:7649–7656.

18. Sirivarasai J, Kaojarern S, Yoovathaworn K, Sura T. Paraoxonase (PON1) polymorphism and activity as the determinants of sensitivity to organophosphates in human subjects. Chem Biol Interact 2007;168:184–192.

19. Aharoni A, Gaidukov L, Yagur S, Toker L, Silman I, Tawfik DS. Directed evolution of mammalian paraoxonases PON1 and PON3 for bacterial expression and catalytic specialization. Proc Natl Acad Sci USA 2004;101:482–487.

20. Amitai G, Gaidukov L, Adani R, Yishay S, Yacov G, Kushnir M, Teitlboim S, Lindenbaum M, Bel P, Khersonsky O, Tawfik DS, Meshulam H. Enhanced stereoselective hydrolysis of toxic organophosphates by directly evolved variants of mammalian serum paraoxonase. FEBS J 2006;273:1906–1919.

21. Yeung DT, Josse D, Nicholson JD, Khanal A, McAndrew CW, Bahnson BJ, Lenz DE, Cerasoli DM. Structure/function analyses of human serum paraoxonase (HuPON1) mutants designed from a DFPase-like homology model. Biochim Biophys Acta 2004;1702: 67–77.

22. SYBYL. Molecular Modelling Software, V7.0. St. Louis, MO: Tripos Associates; 2004.

23. Lee M, Yeh I-C, Zavaljevski N, Wilson P, Reifman J. A software pipeline for protein structure prediction. Proceedings of the 25th Army Science Conference, Orlando, FL, 2006.

24. Sippl MJ. Recognition of errors in three-dimensional structures of proteins. Proteins 1993;17:355–362.

25. Laskowski RA, Macarthur MW, Moss DS, Thornton JM. Procheck—a program to check the stereochemical quality of protein structures. J Appl Crystallogr 1993;26:283–291.

26. Case DA, Darden T, Cheatham TE, III, Simmerling CL, Wang J, Duke RE, Luo R, Merz KM, Wang B, Pearlman DA, Crowley M, Brozell S, Tsui V, Gohlke H, Mongan J, Hornak V, Cui G, Beroza P, Schafmeister C, Caldwell JW, Ross WS, Kollman PA. AMBER 9. San Francisco: University of California; 2006.

27. Ryckaert JP, Ciccotti G, Berendsen JC. Numerical integration of the Cartesian equation of motion of a system with constraints: molecular dynamics of n-alkanes. J Comput Phys 1977;23:327–341.

28. Darden T, York D, Pedersen L. Particle mesh Ewald—an N.Log(N) method for Ewald sums in large systems. J Chem Phys 1993;98: 10089–10092.

29. Berendsen HC, Postma JPM, van Gunsteren WF, DiNole A, Haak J. Molecular dynamics with coupling to an external bath. J Chem Phys 1984;81:3684–3690.

30. Huey R, Morris GM, Olson AJ, Goodsell DS. A semiempirical free energy force field with charge-based desolvation. J Comput Chem 2007;28:1145–1152.

31. Zhang S, Kumar K, Jiang X, Wallqvist A, Reifman J. DOVIS: an implementation for high-throughput virtual screening using AutoDock. BMC Bioinformatics 2008;9:126.

32. Srinivasan J, Miller J, Kollman PA, Case DA. Continuum solvent studies of the stability of RNA hairpin loops and helices. J Biomol Struct Dyn 1998;16:671–682.

33. Kollman PA, Massova I, Reyes C, Kuhn B, Huo S, Chong L, Lee M, Lee T, Duan Y, Wang W, Donini O, Cieplak P, Srinivasan J, Case DA, Cheatham TE, III. Calculating structures and free energies of complex molecules: combining molecular mechanics and continuum models. Acc Chem Res 2000;33:889–897.

34. Onufriev A, Bashford D, Case DA. Modification of the generalized Born model suitable for macromolecules. J Phys Chem B 2000;104: 3712–3720.

35. Sanner MF, Olson AJ, Spehner JC. Reduced surface: an efficient way to compute molecular surfaces. Biopolymers 1996;38:305–320.

36. Massova I, Kollman PA. Computational alanine scanning to probe protein-protein interactions: a novel approach to evaluate binding free energies. J Am Chem Soc 1999;121:8133–8143.